IEEE Photonics Journal
An IEEE Photonics Society Publication

Open Access

Intra-Cavity Chromatic Dispersion Impacts on 10-Gb/s Optical OFDM Transmissions Over 25-km Dual-RSOA-Based Self-Seeded PON Systems

Volume 7, Number 1, February 2015

M. L. Deng
B. Y. Cao
R. P. Giddings
Y. X. Dong
N. Jiang
D. Nesset
K. Qiu
J. M. Tang

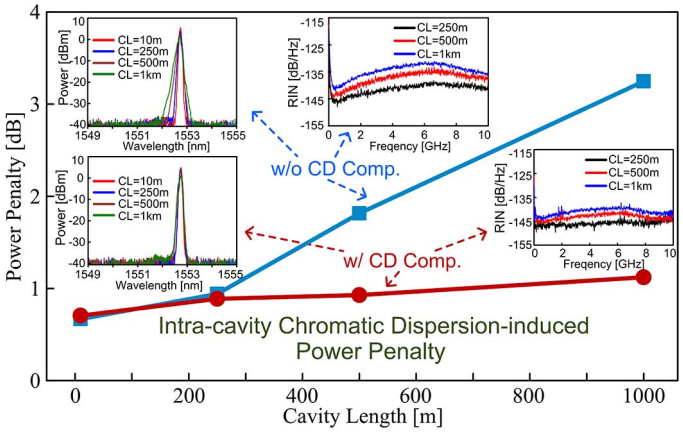

DOI: 10.1109/JPHOT.2014.2381636

Intra-Cavity Chromatic Dispersion Impacts on 10-Gb/s Optical OFDM Transmissions Over 25-km Dual-RSOA-Based Self-Seeded PON Systems

M. L. Deng,[1,2] B. Y. Cao,[2] R. P. Giddings,[2] Y. X. Dong,[2] N. Jiang,[1,2] D. Nesset,[3] K. Qiu,[1] and J. M. Tang[2]

[1]Key Laboratory of Optical Fiber Sensing and Communications, University of Electronic Science and Technology of China, Chengdu 611731, China
[2]School of Electronic Engineering, Bangor University, Bangor LL57 1UT, U.K.
[3]British Telecommunications Laboratories, Martlesham Heath, Ipswich IP5 3RE, U.K.

DOI: 10.1109/JPHOT.2014.2381636

Manuscript received October 22, 2014; revised November 21, 2014; accepted November 21, 2014. Date of publication December 18, 2014; date of current version January 6, 2015. This work was supported in part by the PIANO+ under the European Commission's ERA-NET Plus Scheme within the project OCEAN under Grant Agreement 620029, in part by the Sino-U.K. Higher Education Research Partnership for Ph.D. Studies, the National High Technology Research and Development Program of China (863 Program) (2012AA011302, 2012AA011304, and 2013AA010503), NSFC (61071097, 61107060, and 61101095), and the Fundamental Research Funds for the Central Universities of China (ZYGX2011J009). Corresponding author: J. M. Tang (e-mail: j.tang@bangor.ac.uk).

Abstract: Owing to the lack of strong physical mechanisms capable of elaborately balancing a large number of longitudinal modes created in a self-seeded passive optical network (PON), the resulting coherent-like optical signals are vulnerable to frequency-dependent optical phenomena such as chromatic dispersion (CD). In this paper, based on our recently reported real-time dual-reflective semiconductor optical amplifier (RSOA)-based self-seeded adaptive optical orthogonal frequency-division multiplexing (OOFDM) transmitters, detailed experimental explorations are undertaken, for the first time, of the impacts of intra-cavity CD on 10-Gb/s OOFDM transmissions over 25-km self-seeded PON systems. The cavity length-dependent intra-cavity CD effect is identified to be one of the most prominent physical mechanisms determining the practically achievable performance of such PON systems. In comparison with a 10-m-long dual-RSOA self-seeded fiber cavity, the accumulated intra-cavity CD effect associated with a 1-km-long dual-RSOA self-seeded fiber cavity not only considerably broadens the optical spectral width of the self-seeding-created coherent-like optical signal but increases the signal relative intensity noise (RIN) by 4.8 dB (at a 2-GHz signal spectral region) as well. In addition, a further 1.1-dB signal RIN growth is also measured after the 25-km single-mode fiber (SMF) PON system transmissions. As a direct result, the dual-RSOA self-seeded PON with a 1-km-long fiber cavity suffers from a 2.2-dB power penalty degradation for 10 Gb/s over 25-km SMF intensity modulation and direct detection OOFDM transmissions.

Index Terms: Self-seeded RSOAs, intra-cavity chromatic dispersion, fiber optics systems, orthogonal frequency-division multiplexing (OFDM).

1. Introduction

Due to its' excellent cost-effectiveness, colorlessness, backward compatibility and network flexibility, recent years have seen considerably growing research interest in a self-seeded passive

optical network (PON), where a resonant fiber cavity formed with a reflective semiconductor optical amplifier (RSOA), an optical filter, and a reflective mirror over a part of the PON system produces a self-tunable coherent-like light source, which is directly intensity-modulated and amplified simultaneously by the RSOA located in the optical network unit (ONU) to convey upstream data [1], [2]. Such a self-seeded PON has been experimentally demonstrated to be capable of transmitting multi-gigabits non-return-to-zero on-off keying (NRZ-OOK) upstream signals over relatively long distances [3]–[6]. Recently, 10 Gb/s-class NRZ-OOK signal transmissions have also been reported by making use of 4 GHz modulation bandwidth RSOAs and sophisticated electronic equalizations in the optical line terminal (OLT) [7]. Apart from the abovementioned RSOA-based self-seeded PON transmitters, other PON transmitters incorporated in ONUs have also been reported, which are based on, for example, directly modulated antireflection coated Fabry–Perot laser amplifiers subject to side-mode injection-locking [8] and directly modulated weak-resonant-cavity Fabry-Perot laser diodes [9].

Compared to a conventional semiconductor laser diode, the long fiber cavity of the abovementioned RSOA-based self-seeded PON transmitter accommodates a significantly large number of RSOA amplified spontaneous emission (ASE) noise-initiated longitudinal modes having random phases. This imposes a high relative intensity noise (RIN) on the intensity-modulated optical signal. In addition, a portion of the already intensity-modulated optical signal in the fiber cavity is also reflected, by the mirror, back into the RSOA, the reflected optical signal is then remodulated again by the same RSOA employing an electrical driving signal carrying a different data pattern. Inevitably, this results in the strong residual intensity modulation crosstalk effect. Both the high RIN and strong residual intensity modulation crosstalk effects underpin the utilization of only simple NRZ-OOK modulation formats of large signal extinction ratios in all the aforementioned experimental demonstrations.

Given the fact that commercially available, low-cost RSOAs have very limited signal modulation bandwidths, to further improve the upstream transmission performances of the self-seeded PONs, the adoption of highly spectrally efficient optical orthogonal frequency division multiplexing (OOFDM) is significantly advantageous, which is, however, accompanied with a low signal extinction ratio in typical intensity modulation and direct detection (IMDD) PON systems. To enable the successful utilization of OOFDM, as well as to effectively reduce all the aforementioned unwanted effects associated with the conventional self-seeded PONs, very recently, we have proposed and experimentally demonstrated a face-to-face dual-RSOA-based self-seeded PON [10], in which the reflective mirror incorporated in the conventional self-seeded PON is substituted by a DC-biased RSOA, and the corresponding fiber cavity still consisting of an optical filter is formed with the DC-biased RSOA and a signal-modulated RSOA. The DC-biased RSOA operating at its optical gain saturation region enhances the correlation among various fiber cavity-supported longitudinal modes, and also lowers the residual intensity modulation crosstalk effect. It has been experimentally shown [10] that, in comparison with the conventional self-seeded PONs, an up to 16 dB reduction in RIN and a residual intensity modulation crosstalk suppression of as high as 10.7 dB are obtainable in the proposed dual-RSOA self-seeded PON system. In particular, these features enable the experimental demonstrations of 10 Gb/s over 25 km single mode fiber (SMF) adaptive OOFDM transmissions by making use of two low-cost RSOAs having their modulation bandwidths as small as 1 GHz [10].

However, owing to the lack of strong physical mechanisms capable of elaborately balancing various longitudinal modes in the self-seeded fiber cavity, the intensity and phase of each individual longitudinal mode still fluctuates, to some extent, in both the conventional [11] and dual-RSOA self-seeded fiber cavities. As a direct result, these self-seeded PON systems are vulnerable to frequency-dependent optical phenomena such as chromatic dispersion (CD). To get rid of the CD effect, use has been made of a newly fabricated O-band RSOA chip to enable CD-free upstream signal transmissions at the O-band over the conventional self-seeded PON systems [12]. However, in [12] no detailed investigations have been undertaken of the intra-cavity CD impacts on the PON system performances. In addition, considering the fact that commercially available low-cost RSOAs typically operate in the C-band and that the intra-cavity CD

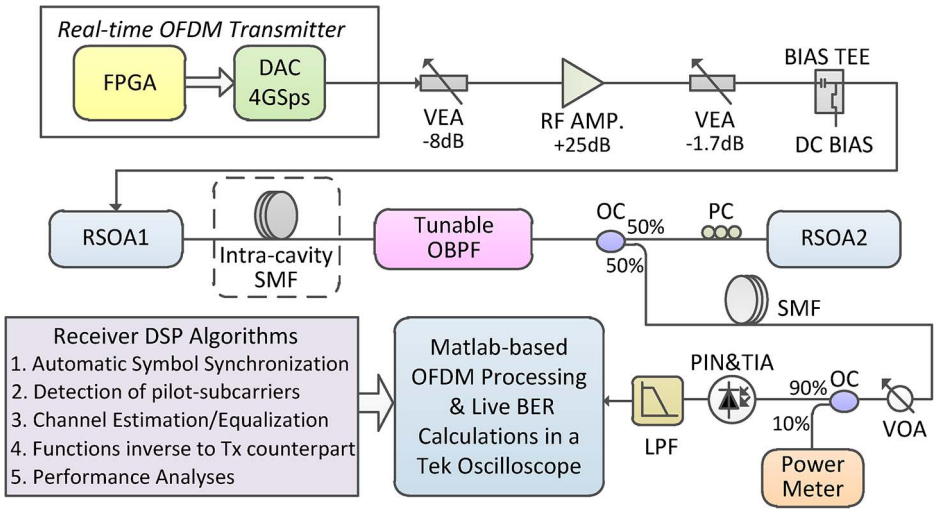

Fig. 1. Experimental system setup of 10 Gb/s over 25 km SMF OOFDM transmissions using the real-time dual-RSOA-based self-seeded transmitter. VEA: variable electrical attenuator; AMP: RF amplifier (10 MHz–4.2 GHz); OBPF: optical band-pass filter; OC: optical coupler; PC: polarization controller; VOA: variable optical attenuator; LPF: low-pass filter (0–2.2 GHz).

characteristics are expected to be different for different variants of the self-seeded cavities, an in-depth understanding of the influence of the accumulated intra-cavity CD effects on the self-seeded PON system performances at the C-band is, therefore, crucial for not only further improving the signal transmission capacity versus reach performance but greatly enhancing the network architecture flexibility as well.

Based on our recently reported real-time face-to-face dual-RSOA-based self-seeded OOFDM transmitters operating at 10 Gb/s [10], the thrust of the present paper is to experimentally explore thoroughly, for the first time, the accumulated intra-cavity CD impacts on 10 Gb/s adaptive OOFDM transmissions over 25 km SMF self-seeded PON systems. The cavity length-dependent intra-cavity CD effect is identified to be one of the most prominent physical mechanisms limiting the practically achievable performance of the PON systems. Our extensive experimental investigations show that, in comparison with a 10 m-long dual-RSOA self-seeded fiber cavity, the accumulated intra-cavity CD effect associated with a 1 km-long dual-RSOA self-seeded fiber cavity not only considerably broadens the optical spectral width of the self-seeding-created coherent-like optical signal but increases the signal RIN by 4.8 dB at a 2 GHz signal spectral region as well. In addition, a further 1.1 dB signal RIN growth is also measured after the 25 km SMF transmissions. As a direct result, the PON system utilizing the 1 km-long dual-RSOA self-seeded fiber cavity suffers from a 2.2 dB power penalty degradation for 10 Gb/s over 25 km SMF adaptive OOFDM PON system transmissions.

2. Experimental Setup of 10 Gb/s Over 25 km Transmission Systems Utilizing a Dual-RSOA Self-Seeded Real-Time OOFDM Transmitter

Fig. 1 shows the adopted entire 10 Gb/s over 25 km SMF IMDD transmission system utilizing the real-time dual-RSOA-based self-seeded OOFDM transmitter, whose physical design architecture and major digital signal processing (DSP) functions incorporated are identical to those reported in [10], except that in Fig. 1 SMFs of various types and lengths are employed inside the fiber cavity to explore the intra-cavity CD effect. The key transceiver component and system parameter values employed in the experimental system are presented in Table 1.

At the transmitter side, the real-time OOFDM transmitter consists of a 4 GS/s@8-bit digital-to-analogue converter (DAC) and a field programmable gate array (FPGA) for performing high-speed transmitter DSP functionalities including pseudo-random data generation; online adaptive

TABLE 1

OOFDM transceiver and PON system parameters

Parameter	*Value*	*Units*
Total number of IFFT/FFT points per symbol	32	
Data-carrying subcarriers per symbol	15	
n-th subcarrier frequency	*n*×125	MHz
Adaptive modulation formats on all subcarriers	16-QAM, 32-QAM or 64-QAM	
DAC (ADC) sample rate	4 (6.25)	GS/s
DAC(ADC) resolution	8 (8)	bits
OFDM symbol rate	100	GS/s
Samples per symbol	32 samples (8ns)	
Cyclic prefix	8 samples (2ns)	
Total samples per symbol	40 samples (10ns)	
Error calculation period	4000 symbols	
Total raw signal bit rate	10	Gb/s
OFDM electrical bandwidth	2	GHz
RSOA1 (RSOA2) operating wavelength	1550 (1550)	nm
RSOA1 (RSOA2) small signal gain (50mA, 20°C)	20(30)	dB
RSOA1 (RSOA2) polarization dependent gain	0.4 (24)	dB
RSOA1 (RSOA2) bias current	80 (95)	mA
RSOA1 (RSOA2) operating temperature	13 (16)	°C
RSOA1 (RSOA2) saturated output power (50mA, 20°C)	1.6(3.5)	dBm
RSOA1 modulation bandwidth (3dB)	1.125	GHz
RSOA1 driving voltage	3.2	V_{pp}
OBPF bandwidth	1.2	nm
OBPF insertion loss	1.9	dB
Fiber cavity length	10, 250, 500, 1000	m
SMF type inside the cavity	MetroCor/LEAF	
Optical launch power	~5	dBm
PIN detector bandwidth	12	GHz
PIN detector sensitivity[1]	-19	dBm
SMF type over transmissions	MetroCor	
Transmission distance	25	km
MetroCor (LEAF) dispersion value (1550nm)	-6.8 (6.5)	ps/nm/km
MetroCor (LEAF) attenuation value (1550nm)	0.2 (0.19)	dB/km

[1] Corresponding to 10 Gb/s non-return-to-zero data (PRBS 2^{31}-1) at a BER of 1.0×10^{-9}

bit and power loading for 125 MHz-spaced 15 data-carrying subcarriers with signal modulation formats ranging from 16-quadrature amplitude modulation (QAM) to 32-QAM and to 64-QAM; pilot-tone insertion; a 32-point inverse fast Fourier transform (IFFT) to generate real-valued time-domain digital OFDM symbols at 100 MHz; addition of 25% cyclic prefix (CP); online signal clipping level adjustment, and 8-bit sample quantization. Full descriptions of the FPGA-based OFDM transmitter design and corresponding DSP algorithms can be found in [13] and [14]. Utilizing the FPGA embedded memory editor via a joint test action group (JTAG) connection to a personal computer, the above-mentioned transmitter DSP designs offer live optimizations of both the subcarrier bit/power allocation and the digital signal clipping level.

As shown in Fig. 1, after the optimization of the electrical signal power level using two variable electrical attenuators together with a 4.2 GHz RF amplifier in-between, the analog electrical OFDM signal is then combined with an 80 mA DC bias current in a 6 GHz bias tee to directly modulate a polarization-insensitive RSOA operating at a temperature of 13 °C. Throughout the paper, the electrical signal modulated RSOA is referred to as RSOA1. The output optical signal from RSOA1 passes through intra-cavity SMFs and a tunable optical band-pass filter (OBPF) which initially selects an operation wavelength. At the 50/50 optical coupler (OC), the incident optical power is split into two portions: one portion is first fed to a polarization controller (PC), then amplified and reflected by a DC-biased polarization-sensitive RSOA operating at its' optical gain saturation region and a temperature of 16 °C, the portion is finally fed back to RSOA1 for remodulation; whilst the other portion is launched into a 25 km SMF IMDD PON transmission

system without inline optical amplification and dispersion compensation. Throughout the paper, the DC-biased RSOA is termed RSOA2. The PC prior to RSOA2 is employed to align the optical signal polarization state with the high gain polarization state of the polarization-sensitive RSOA2. The utilization of the temperature control for both RSOAs is to ensure that these RSOAs operate at their optimum conditions within their manufacturer-specified temperature ranges, corresponding to which the maximum transmission performances are obtainable.

To experimentally explore the impacts of the accumulated intra-cavity CD effect on the transmission performance of the dual-RSOA-based self-seeded PON system, two types of fibers of various lengths in the fiber cavity are employed with all other PON system components and their parameters kept unchanged. For all experimental cases without intra-cavity CD compensation, here referred to as the dispersive cavity, MetroCor fibers of various lengths are utilized only; whilst for all experimental cases with intra-cavity CD compensation, here referred to as the CD-compensated cavity, MetroCor and large effective area fibers (LEAFs) of same lengths are adopted to enable the complete CD compensation within the self-seeded cavities, as their dispersion parameters are of the opposite signs and similar absolute values, as presented in Table 1. On the other hand, since the attenuation coefficients of the MetroCor and LEAF fibers are almost identical, both the dispersive and CD-compensated cavities of the same lengths have almost identical total intra-cavity losses. Such self-seeded fiber cavity designs allow fair performance characteristic comparisons, based on which the impacts of the accumulated intra-cavity CD effect can be identified easily for various scenarios of interest of the present paper.

At the receiver side, the optical signal first passes through a variable optical attenuator to control the received optical power, and then a 12 GHz PIN+TIA performs the optical-to-electrical conversion of the received OOFDM signal. After having been filtered by a 2.2 GHz electrical low pass filter, the received analog OFDM signal is captured and digitized by a real-time sampling oscilloscope and finally processed using Matlab. Similar to those reported in [13] and [14], the receiver DSP procedures include symbol synchronization, pilot-subcarrier detection, channel estimation/equalization, and all other receiver DSP functions that are just inverse to their transmitter counterparts. Bit error rates (BERs) of each individual subcarrier and the entire OFDM channel are continuously calculated and displayed in the oscilloscope. This enables the rapid optimization of the overall PON systems via component/system parameter adjustments including adaptive subcarrier bit and power loading.

Here it is also worth addressing, in particular, the following two aspects: a) For the dispersive and CD-compensated cavities of various lengths ranging from 10 m to 1 km, their total intra-cavity loss variations are too small to considerably affect the operating conditions of both RSOA1 and RSOA2; b) It is well known that the accumulated CD effect is proportional to fiber length, however the exact number of round-trips of optical signal propagation within the self-seeded cavity prior to the optical signal's departure from the cavity is unknown. To easily quantify the cavity length-dependent intra-cavity CD impacts, relevant measured performances are, therefore, plotted as a function of cavity length, as presented in Section 3.

3. Experimental Results and Discussions

In Sections 3.1 and 3.2, for different PON system configurations, extensive experimental explorations are undertaken of the cavity length-dependent optical spectral and RIN characteristics of the dual-RSOA-based self-seeding-generated coherent-like light sources. An insight of these dynamic characteristics lays a solid foundation for gaining a better understanding of the overall system performances, and more importantly, for identifying the key limiting factors' contributions to the PON performance degradations discussed in Section 3.3.

3.1. Intra-Cavity CD-Induced Optical Spectral Broadening

For the dispersive and CD-compensated cavities of different lengths, their optical spectra measured at the 50/50 optical coupler indicated in Fig. 1 are shown in Fig. 2, where the frequency response of the adopted OBPF is also plotted in each figure. In obtaining Fig. 2,

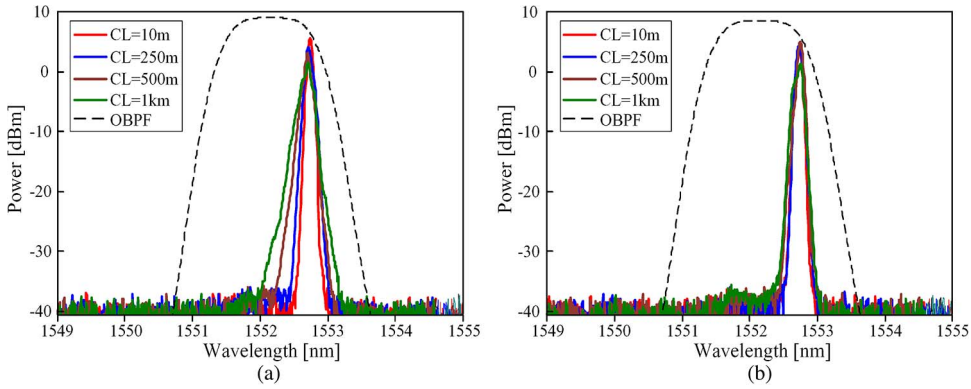

Fig. 2. Measured output optical spectra for different dual-RSOA-based self-seeded fiber cavity lengths. The measured frequency response of the adopted OBPF is also shown in each figure. (a) Output optical spectra from dispersive cavities. (b) Output optical spectra from CD-compensated cavities. CL: cavity length.

RSOA1 and RSOA2 are biased at fixed DC currents of 80 mA and 95 mA, respectively, and no OFDM driving currents are applied to RSOA1.

It can be seen in Fig. 2(a) that, the output optical spectral width considerably broadens for a long dispersive cavity. This agrees well with theoretical simulations reported in [11]. In sharp contrast to Fig. 2(a), for the CD-compensated cavities, their output spectral profiles seen in Fig. 2(b) are almost independent of cavity length and nearly identical to that corresponding to the shortest cavity length of 10 m. This indicates that the accumulated intra-cavity CD effect is a dominant factor responsible for the spectral broadening observed in the dispersive cavities. The intra-cavity CD effect messes up the delicate phase relationships between various cavity-supported longitudinal modes, thus weakens the mode competition and subsequently leads to a wide output optical spectrum with more longitudinal modes survived. It should also be noted that the spectral broadening not only further degrades the tolerance of the intensity-modulated optical signals to the CD impairments over signal transmissions in the PON systems, but also contributes to the intra-cavity CD-induced RIN growth at the outputs of both the self-seeded cavities and PON transmission systems, as discussed in Section 3.2.

3.2. Intra-Cavity CD-Induced RIN Increase

Throughout the present paper, to experimentally measure the dynamic RIN characteristics, a real-time oscilloscope is first employed to capture and subsequently digitize the detector noise and the received signal separately. Then the Welch's averaged modified periodogram method with a Hamming window is utilized to obtain the power spectral density of the signal. Having subtracted the detector noise from the signal power spectral density, the resulting power spectral density is then normalized utilizing the average optical power calculated by considering the detector responsivity. Thus the RIN spectrum satisfying its' conventional definition is achieved. Figs. 3(a) and 4(a) show the RIN spectra measured at the outputs of the dispersive and CD-compensated cavities of various lengths, respectively. For three representative frequencies of 0.5 GHz, 1 GHz, and 2 GHz, which correspond to the low, middle and high frequencies of the OFDM signal spectral regions, Figs. 3(b) and 4(b) show that the RIN characteristics are cavity length-dependent. The RIN increase in Fig. 3(b) is defined as the ratio between the RIN measured for a considered cavity length and the RIN corresponding to the 10 m-long cavity length, whilst the RIN reduction in Fig. 4(b) is defined as the RIN difference between the dispersive cavity and the CD-compensated cavity with the same cavity lengths. In obtaining both Figs. 3 and 4, RSOA1 and ROSA2 operating conditions are identical to those adopted in Fig. 2.

It is shown in Fig. 3(a) and (b) that the RIN quickly increases with increasing dispersive cavity length. Such cavity length-dependent RIN behaviors are mainly attributed to the following three physical mechanisms: a) the augmented mode partition noise due to the long cavity-induced

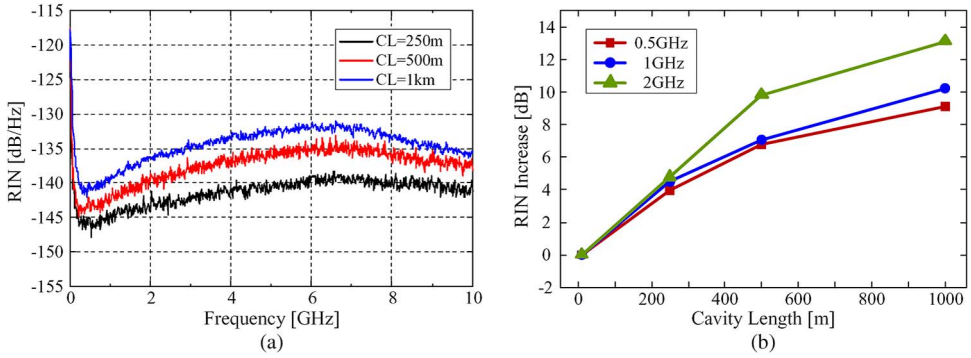

Fig. 3. Measured RIN characteristics at outputs of dispersive cavities. (a) RIN spectra for various cavity lengths. (b) Cavity length-dependent RIN increases at representative frequencies. CL: cavity length.

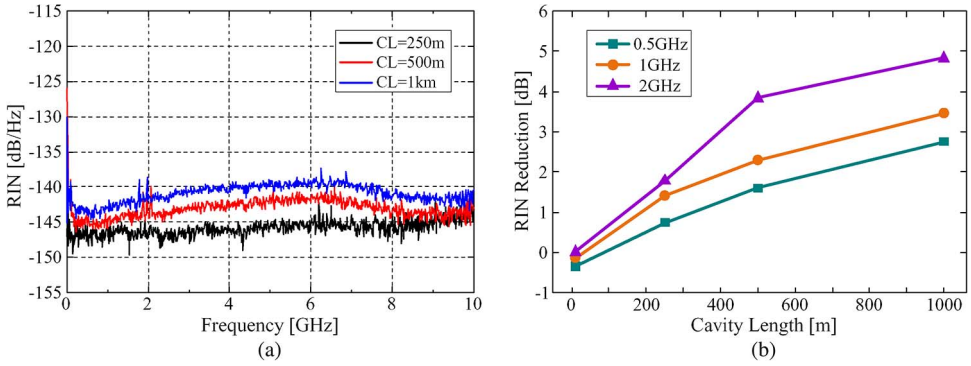

Fig. 4. Measured RIN characteristics at outputs of CD-compensated cavities. (a) RIN spectra for various cavity lengths. (b) Cavity length-dependent RIN reductions at representative frequencies. CL: cavity length.

growth in the number of longitudinal modes [12]; (b) strong longitudinal mode phase mismatches caused by the long cavity-enhanced intra-cavity CD effect; and (c) long cavity-associated optical spectral broadening presented in Section 3.1. As seen in Fig. 3(b), when the cavity length is extended from 10 m to 1 km, a RIN increase can be as high as 13.2 dB at 2 GHz, the signal frequency-dependent RIN is because of the high-pass filtering effect resulting from the gain-saturated RSOAs [10].

In comparison with the dispersive cavities, for the CD-compensated cavities, the RINs decrease considerably for all the cases considered, as depicted in Fig. 4(a), where the existence of the residual RIN differences between different cavity lengths is mainly due to different cavity length-associated mode partition noise and the imperfect intra-cavity CD compensation. More importantly, it is shown in Fig. 4(b) that the intra-cavity CD compensation-induced RIN reduction increases with both cavity length and signal frequency. For instance, a 4.8 dB RIN reduction at 2 GHz is feasible for the 1 km-long cavity. The above results confirm that the accumulated intra-cavity CD effect plays an important role in determining the optical signal RIN dynamics at the outputs of the self-seeded cavities.

Furthermore, the 25 km SMF IMDD transmission can increase the optical signal RIN at 1 GHz by about 3.2 dB for the dispersive cavities of different lengths, as shown in Fig. 5, where the RIN differences between the RIN level measured in the OLT receiver after the PON transmission and the RIN level measured at the output of the corresponding self-seeded cavity are plotted as a function of transmission distance. It can also be seen in Fig. 5 that, in comparison with the dispersive cavities, for the 25 km SMF IMDD transmission, the CD-compensated cavities

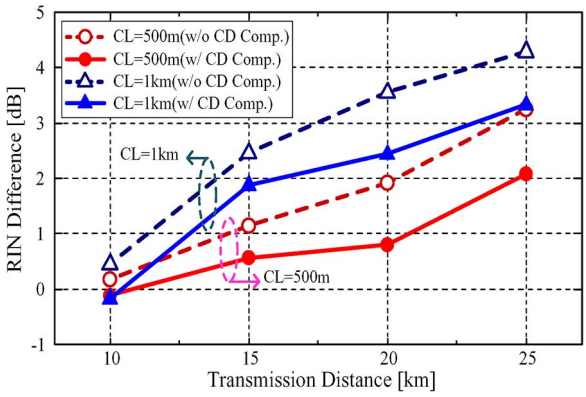

Fig. 5. Transmission distance-dependent RIN differences between the RIN measured after the transmission in the OLT receiver and the RIN measured at the output of the self-seeded cavity. Here, a middle signal frequency of 1 GHz is chosen. CL: cavity length.

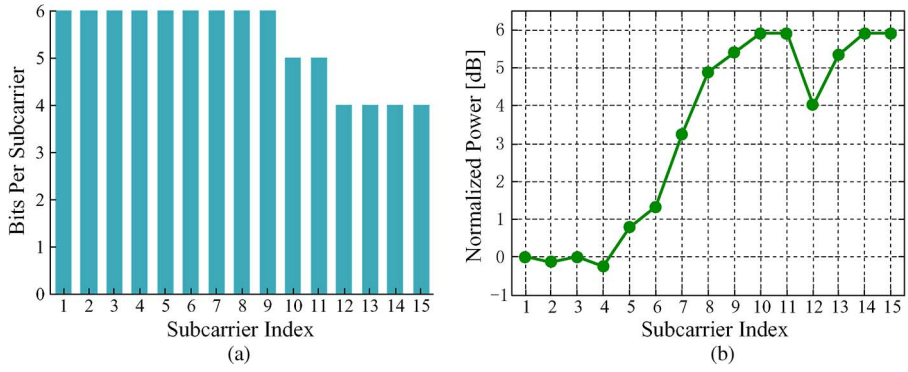

Fig. 6. (a) Optimum subcarrier bit loading profile. (b) Adaptively loaded subcarrier power profile which is normalized to the first subcarrier power.

decrease the transmission-induced signal RIN growth by 1.1 dB, regardless of the cavity lengths. Similar to those reported for multi-longitudinal mode lasers [15] and spectrally sliced ASE light sources with RIN suppression [16], [17], it is shown in Fig. 5 that the RIN difference grows rapidly with increasing transmission distance. This mainly results from transmission system CD-induced temporal walk-off between different longitudinal modes. Moreover, as a direct result of a long cavity-induced increase in the number of longitudinal modes, the intra-cavity CD effect associated with a long dispersive self-seeded cavity gives rise to a fast growing RIN difference for transmission distances of $>$ 10 km, as demonstrated in Fig. 5.

3.3. Intra-Cavity CD Impacts on PON System Performances

This subsection is to experimentally explore the intra-cavity CD impacts upon transmission performances of 10 Gb/s OOFDM signals over 25 km SMF IMDD PON systems in terms of BER and power penalty. In measuring the results presented in the subsection, the OOFDM transceiver and system parameters listed in Table 1 are employed. To effectively compensate for the overall system frequency response roll-off effect [18] and simultaneously improve the adaptive OOFDM transmission performance, parameter optimizations are first conducted via adaptive bit and power loading on the 15 information-bearing subcarriers. Fig. 6(a) illustrates the obtained optimum bit loading profile, based on which the raw signal bit rate of 10 Gb/s can be easily worked out utilizing the transceiver parameters listed in Table 1. It is also shown in Fig. 6(a) that low signal modulation formats occur on high frequency subcarriers, which are mainly attributed to the electrical components involved in the transmitter [18]. On the other

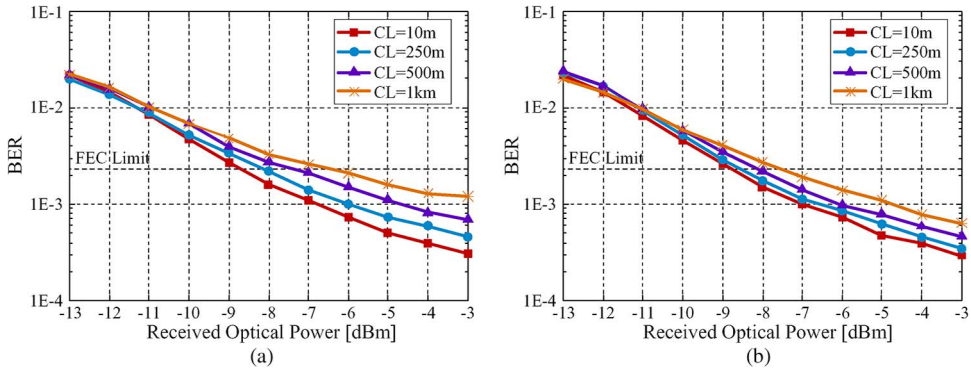

Fig. 7. Measured BER versus received optical power performances for optical BTB system configurations. (a) Dispersive cavities of various lengths. (b) CD-compensated cavities of various lengths. CL: cavity length.

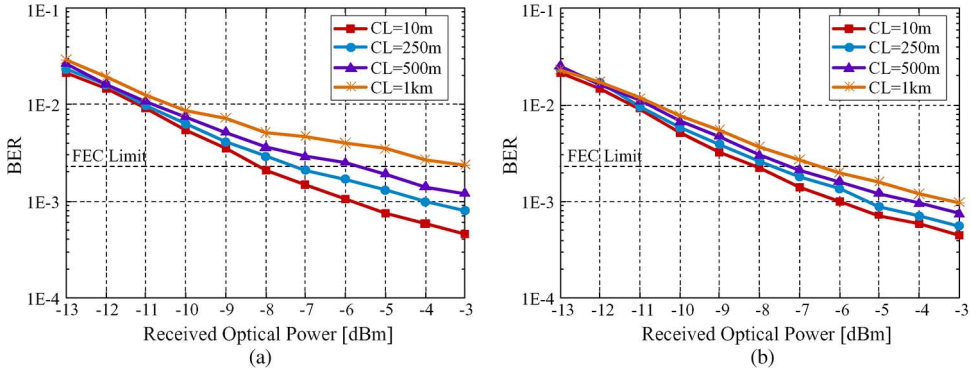

Fig. 8. Measured BER versus received optical power performances after 25 km SMF IMDD transmissions. (a) Dispersive cavities of various lengths. (b) CD-compensated cavities of various lengths. CL: cavity length.

hand, the resulting optimum subcarrier power loading profile is given in Fig. 6(b), where the existence of a power dip for high frequency subcarriers is due to the water-filling optimization process. It should be pointed out that the variations in the types of self-seeded cavities and their corresponding cavity lengths do not alter the aforementioned optimum bit and power loading profiles.

By making use of the optimum bit and power loading profiles presented in Fig. 6, Figs. 7 and 8 show the measured BER performances for 10 Gb/s adaptive OOFDM signal transmissions for these two cavity types of various lengths for both the optical back-to-back (BTB) and the 25 km SMF IMDD system configurations, respectively. In Fig. 7(a), it can be clearly seen that the system BER performance degrades as the dispersive cavity length increases. When the cavity length is extended from 10 m to 1 km, the minimum total channel BER is increased from 3×10^{-4} to 1.2×10^{-3} at the received optical power of -3 dBm. In particular, such a cavity length variation results in a 2.6 dB reduction in receiver sensitivity at the forward error correction (FEC) limit of 2.3×10^{-3} [19]. The measured receiver sensitivity degradation can be easily understood by considering the intra-cavity CD-induced optical signal RIN increase presented in Section 3.2. As a direct result of intra-cavity CD compensation, the CD-compensated cavities with their lengths varying within the same dynamic range correspond to a receiver sensitivity degradation of as low as 1.5 dB, as illustrated in Fig. 7(b). Such remaining receiver sensitivity difference is mainly because of the imperfect intra-cavity CD compensation and cavity length-associated mode partition noise.

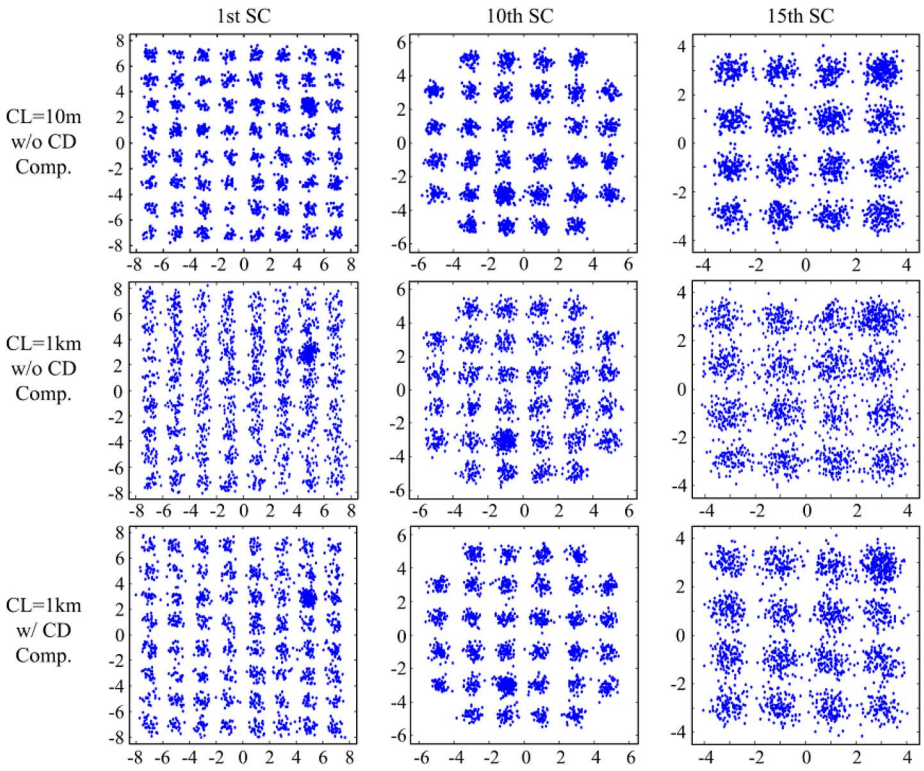

Fig. 9. Received constellations of representative subcarriers after performing channel equalization for 25 km SMF IMDD transmissions at received optical powers of −3 dBm. CL: cavity length.

As expected from discussions in Section 3.2, Fig. 8(a) shows that 25 km SMF IMDD OOFDM signal transmissions result in more severe BER performance degradations for the dispersive cavities, and an error floor-like BER developing trend at received optical powers of > -4 dBm begins to occur for the 1 km-long dispersive cavity. However, such a BER developing trend completely disappears for the 1 km-long CD-compensated cavity, as shown in Fig. 8(b), this gives rise to a 3.4 dB improvement in receiver sensitivity compared to the 1 km-long dispersive cavity. In addition, it is also very interesting to note that, in Fig. 8(b) for cavity lengths varying from 10 m to 1 km, the receiver sensitivity difference is almost identical to that observed in Fig. 7(b) for the BTB case, this is in good agreement with Fig. 5.

After performing channel equalization in the receiver, for both the dispersive and CD-compensated cavities of different lengths, the measured constellations of the 1st, 10th, and 15th subcarriers are exemplified in Fig. 9, which are recorded at received optical powers of −3 dBm after the 25 km SMF IMDD transmissions. As expected from Fig. 8(a) and (b), for these representative subcarriers, the 10 m-long dispersive cavity has relatively clean constellation diagrams, which become very noisy when the cavity length is extended to 1 km. On the other hand, the 1 km-long CD-compensated cavity has considerably improved constellation diagrams for all the subcarriers.

To further demonstrate explicitly the accumulated intra-cavity CD impact upon the PON system performance, for both the dispersive and CD-compensated cavities, the cavity length-dependent power penalties for 10 Gb/s over 25 km OOFDM transmissions are given in Fig. 10, where the power penalty values corresponding to the above-mentioned FEC limit are obtained by extracting the experimentally measured results presented in Figs. 7 and 8. As expected from the discussions in Section 3.2, it can be easily seen in Fig. 10 that for the dispersive cavity, the power penalty in dB is almost proportional to cavity length, whilst the power penalty curve is significantly flattened for the CD-compensated cavity. For example, an increase in dispersive cavity

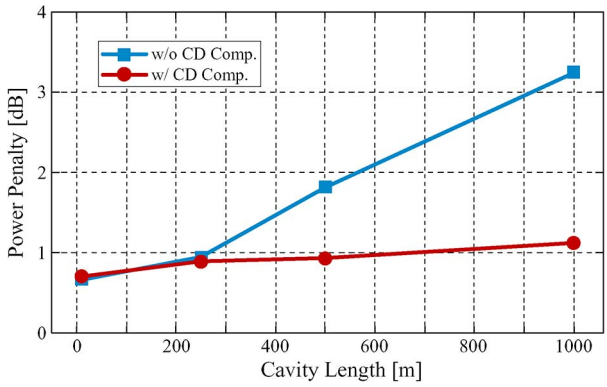

Fig. 10. Power penalty versus self-seeded cavity length for both the dispersive and CD-compensated cavities after 10 Gb/s over 25 km SMF signal transmissions.

length from 10 m to 1 km gives rise to a power penalty increase of as high as 2.6 dB, which is, however, reduced to a value of as small as 0.4 dB when the CD-compensated cavities are adopted. This indicates that, for a 1 km-long self-seeded cavity, the accumulated intra-cavity CD effect alone can cause a power penalty increase of as large as 2.2 dB for 10 Gb/s over 25 km IMDD OOFDM transmissions.

4. Conclusion

By making use of our recently reported real-time 10 Gb/s face-to-face dual-RSOA-based self-seeded OOFDM transmitters, detailed experimental investigations have been conducted, for the first time, the impacts of the accumulated intra-cavity CD effect on the transmission performances of the 25 km IMDD dual-RSOA-based self-seeded PON systems. The cavity length-dependent intra-cavity CD effect has been identified to be one of the most prominent physical mechanisms limiting the practically achievable performance of the PON systems. In comparison with a 10 m-long fiber cavity, the accumulated intra-cavity CD effect associated with a 1 km-long fiber cavity not only considerably broadens the optical spectral width, but also increases the signal RIN by 4.8 dB at a 2 GHz spectral region. In addition, a further 1.1 dB signal RIN growth is also measured after 25 km SMF IMDD transmission. Our experimental results have also shown that, for the 1 km-long fiber cavity, the intra-cavity CD effect can give rise to a 2.2 dB increase in power penalty for 10 Gb/s over 25 km SMF IMDD transmission systems. The present work provides an in-depth understanding of the dynamic intra-cavity CD influence on the transmission performance of the dual-RSOA-based self-seeded PON systems, this is valuable for practically designing optimum self-seeded PON systems enabling improved transmission performances and enhanced architecture flexibility.

To improve the transmission performance of the self-seeded PON systems through intra-cavity CD compensation, in practice, use may be made of the following two approaches: a) For transmission systems with known operation parameters, advanced DSP algorithms implemented in the transmitter and/or receiver may be adopted to digitally compensate for the CD-induced impairments in the electrical domain, and b) in the optical domain, the shape of the involved OBPF frequency response may be appropriately engineered to compensate for the intra-cavity CD effect.

References

[1] E. Wong, K. L. Lee, and T. B. Anderson, "Directly modulated self-seeding reflective semiconductor optical amplifiers as colorless transmitters in wavelength division multiplexed passive optical networks," *J. Lightw. Technol.*, vol. 25, no. 1, pp. 67–74, Jan. 2007.

[2] M. Presi and E. Ciaramella, "Stable self-seeding of R-SOAs for WDM-PONs," in *Proc. OFC/NFOEC*, Los Angeles, CA, USA, 2011, pp. 1–3.

[3] L. Marazzi, P. Parolari, R. Brenot, G. de Valicourt, and M. Martinelli, "Network-embedded self-tuning cavity for WDM-PON transmitter," *Opt. Exp.*, vol. 20, no. 4, pp. 3781–3786, Feb. 2012.
[4] F. Xiong *et al.*, "Characterization of directly modulated self-seeded reflective semiconductor optical amplifiers utilized as colorless transmitters in WDM-PONs," *J. Lightw. Technol.*, vol. 31, no. 11, pp. 1727–1733, Jun. 2013.
[5] Q. Deniel, F. Saliou, P. Chanclou, D. Erasme, and R. Brenot, "Up to 45 km-long amplified self-seeded RSOA based external cavity for 2.5 Gb/s WDM PON transmission," in *Proc. OFC/NFOEC*, Anaheim, CA, USA, 2013, pp. 1–3.
[6] Q. Deniel, F. Saliou, P. Chanclou, and D. Erasme, "Self-seeded RSOA based WDM-PON transmission capacities," in *Proc. OFC/NFOEC*, Anaheim, California, USA, 2013, pp. 1–3.
[7] L. Marazzi *et al.*, "Up to 10.7-Gb/s high-PDG RSOA-based colorless transmitter for WDM networks," *IEEE Photon. Technol. Lett.*, vol. 25, no. 7, pp. 637–640, Apr. 2013.
[8] G.-R. Lin *et al.*, "Long-cavity Fabry-Perot laser amplifier transmitter with enhanced injection-locking bandwidth for WDM-PON application," *J. Lightw. Technol.*, vol. 28, no. 20, pp. 2925–2932, Oct. 2010.
[9] G.-R. Lin *et al.*, "200-GHz and 50-GHz AWG channelized linewidth dependent transmission of weak-resonant-cavity FPLD injection-locked by spectrally sliced ASE," *Opt. Exp.*, vol. 17, no. 20, pp. 17 739–17 746, Sep. 2009.
[10] M. L. Deng *et al.*, "Self-seeding-based 10 Gb/s over 25 km optical OFDM transmissions utilizing face-to-face dual-RSOAs at gain saturation," *Opt. Exp.*, vol. 22, no. 10, pp. 11 954–11 965, May 2014.
[11] S. A. Gebrewold *et al.*, "Reflective-SOA fiber cavity laser as directly modulated WDM-PON colorless transmitter," *IEEE J. Sel. Top. Quantum Electron.*, vol. 20, no. 5, Sep./Oct. 2014, Art. ID. 3100409.
[12] P. Parolari *et al.*, "10-Gb/s operation of a colorless self-seeded transmitter over more than 70 km of SSMF," *IEEE Photon. Technol. Lett.*, vol. 26, no. 6, pp. 599–602, Mar. 2014.
[13] R. P. Giddings *et al.*, "Experimental demonstration of a record high 11.25 Gb/s real-time optical OFDM transceiver supporting 25 km SMF end-to-end transmission in simple IMDD systems," *Opt. Exp.*, vol. 18, no. 6, pp. 5541–5555, Mar. 2010.
[14] X. Q. Jin *et al.*, "Experimental demonstrations and extensive comparisons of end-to-end real-time optical OFDM transceivers with adaptive bit and/or power loading," *IEEE Photon. J.*, vol. 3, no. 3, pp. 500–511, Jun. 2011.
[15] X. Lu, C. B. Su, R. B. Lauer, G. J. Meslener, and L. W. Ulbricht, "Analysis of relative intensity noise in semiconductor lasers and its effect on subcarrier multiplexed lightwave systems," *J. Lightw. Technol.*, vol. 12, no. 7, pp. 1159–1166, Jul. 1992.
[16] H. Kim, S. Kim, S. Hwang, and Y. Oh, "Impact of dispersion, PMD, and PDL on the performance of spectrum-sliced incoherent light sources using gain-saturated semiconductor optical amplifiers," *J. Lightw. Technol.*, vol. 24, no. 2, pp. 775–785, Feb. 2006.
[17] S.-H. Cho *et al.*, "Loop-back WDM-PON with 100 Gb/s capacity using spectrally sliced ASE injected RSOA," *J. Opt. Commun. Netw.*, vol. 5, no. 5, pp. 447–456, 2013.
[18] R. P. Giddings, E. Hugues-Salas, X. Q. Jin, J. L. Wei, and J. M. Tang, "Experimental demonstration of real-time optical OFDM transmission at 7.5 Gb/s over 25-km SSMF using a 1-GHz RSOA," *IEEE Photon. Technol. Lett.*, vol. 22, no. 11, pp. 745–747, Jun. 2010.
[19] X. Q. Jin *et al.*, "First real-time experimental demonstrations of 11.25 Gb/s optical OFDMA PONs with adaptive dynamic bandwidth allocation," *Opt. Exp.*, vol. 19, no. 21, pp. 20 557–20 570, Oct. 2011.